Fingerprint Minutiae Matching Through Sparse Cross-correlation

Gabriel Emile Hine, Emanuele Maiorana, Patrizio Campisi
Section of Applied Electronics, Engineering Department,
Università degli Studi Roma Tre
Email: {gabriel.hine,emanuele.maiorana,patrizio.campisi}@uniroma3.it

***Abstract*—In this paper, we introduce a novel minutiae-based matching algorithm for fingerprint recognition. The method is built on an elegant and straightforward mathematical formulation: the minutiae set is represented by a train of complex pulses and the matching algorithm is based on a simple cross-correlation. We propose two different implementations. The first one exploits the intrinsic sparsity of the signal representing the minutiae set in order to construct an efficient implementation. The other relies on the Fourier transform to build a fixed-length representation, being thus suitable to be used in many biometric crypto-systems. The proposed method exhibits performance comparable with NIST's Bozorth3, that is a standard *de facto* for minutiae matching, but it shows to be more robust with cropped fingerprints.**

I. Introduction

Fingerprints are the most-used biometric traits thanks to their usability, low-cost, and accuracy. The minutiae-based techniques [1] are nowadays the consolidated matching methods, due to their high performance and low computational memory requirements. Nevertheless, they still show some weaknesses: mainly, the variability of the length of the representation and the drop of recognition rate in the cropped images scenario, due for example to the small size of the acquisition sensors of mobile devices.

The variability of the length of the representation makes the system incompatible with the majority of biometric crypto-system methods [2]–[4]. There is indeed a big effort from the community to find novel fixed-length representations of fingerprints [5], [6]. The problem with these representations is that they incur a significant drop in recognition accuracy. Some attempts to build fixed-length representations directly from minutiae have been proposed, such as the spectral minutia representation [5] or minutia cylinder-code (MCC) [7]. The MCC method is not truly a fixed-length representation since some of its cells may be invalid, and the amount of invalid cells is unpredictable. The Spectral Minutia Representation suffers from poor recognition rates. This is mainly due to their minutiae representation that, with the aim of achieving translation invariance, gets rid of a large amount of useful information. This aspect will be extensively discussed in Section II-A.

Regarding the drop of performance when dealing with partial fingerprint images, usually, additional features are taken from the fingerprint image [8]–[10]. These techniques are more computationally expensive because they usually apply cross-correlation or similar operations directly to the fingerprint images. Furthermore, the use of additional features to ISO/IEC 19794 standard minutiae goes against interoperability.

In this work, we take inspiration from the fundamentals at the basis of the spectral minutia representation approach [5] to arrange minutiae sets in such a way they can be treated with signal processing techniques. In more details, minutiae are represented by a sparse complex signal and the matching is based on a simple cross-correlation. Since no hard decision is taken on corresponding minutia couples, the system is more robust to the missing-minutiae scenario. The sparsity of the signal makes the cross-correlation computation very fast. Furthermore, all operations can be implemented also in the frequency domain by means of a fixed-length representation.

In Section II-A, we will give some remarks on the representation proposed in [5] and discuss its limitation. In Section II-B we will show how to exploit the sparsity of the minutiae signal representation to design a very elegant, accurate and fast matching algorithm based on spatial-domain analytical cross-correlation. In Section II-C, a spectral representation of the same algorithm will be shown. Eventually, experimental results will be shown in Section III.

II. Complex domain minutia representation

Let $M = m_i : \{x_i, y_i, \alpha_i | i = 1, ..., N\}$ be an unordered set of minutiae where x and y are the Cartesian coordinates and α is the orientation of the minutia. As suggested in [5], [11], [12], each minutia m_i can be represented as an isotropic Gaussian function centred in (x_i, y_i) whose amplitude is modulated by $e^{\iota\alpha}$. Therefore, a minutiae set can be represented as a mixture of Gaussian functions:

$$\begin{aligned} M(x,y) &= \sum_{i=1}^{N} e^{\iota\alpha_i} \frac{1}{2\pi\sigma^2} e^{\frac{-\left[(x-x_i)^2+(y-y_i)^2\right]}{2\sigma^2}} = \\ &= \frac{1}{2\pi\sigma^2} e^{\frac{-(x^2+y^2)}{2\sigma^2}} * \sum_{i=1}^{N} e^{\iota\alpha_i} \delta(x - x_i, y - y_i), \end{aligned} \tag{1}$$

where $\delta(\cdot,\cdot)$ represents the Dirac distribution and $*$ the convolution operator. The σ parameter is meant to absorb the variability of the relative location of minutiae due to potential fingerprint distortion. This formulation has been shown to be very useful to generate a fixed-length representation in the spectral domain [5], [11], [12].

ISBN 978-90-827970-1-5

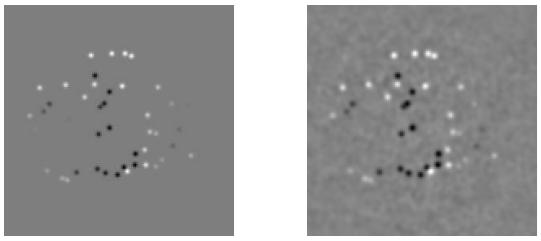

(a) Original Signal

(b) Reconstruction with phase only spectrum information

Fig. 1. Real part of the Minutiae complex representation $\mathscr{R}e\{M(x,y)\}$

A. Some Remarks on the Spectral Minutiae Representation

In [5], [11], [12], the authors use as a template the absolute value of spectral representation of the minutiae set $|\mathscr{M}(\omega_x,\omega_y)|$, discarding the phase information, thus making the template invariant to spatial translation.

$$\begin{aligned}\mathscr{M}(\omega_x,\omega_y) &= \int\int M(x,y)e^{-\iota(\omega_x x+\omega_y y)}dxdy = \\ &= e^{-(\omega_x^2+\omega_y^2)\frac{\sigma^2}{2}}\sum_{i=1}^{N} e^{-\iota(\omega_x x_i+\omega_y y_i)}e^{-\iota\alpha_i}\end{aligned} \tag{2}$$

However, it is well known that the phase removal induces significant loss of information that is useful for the recognition process. As an example, in Figure 1 the original representation $M(x,y)$ and the one reconstructed when discarding the magnitude of the spectral representation (3) are shown.

$$\mathscr{F}^{-1}\left\{e^{-(\omega_x^2+\omega_y^2)\frac{\sigma^2}{2}}\frac{\mathscr{M}(\omega_x,\omega_y)}{|\mathscr{M}(\omega_x,\omega_y)|}\right\} \tag{3}$$

By looking the figure, it is clear that the phase data alone contain almost all the information.
Furthermore, let's take into account two minutiae sets $M^{(a)}$ and $M^{(b)}$. Let's suppose

$$x_i^{(a)} = x_i^{(b)},\ y_i^{(a)} = y_i^{(b)},\ \alpha_i^{(a)} = \alpha_i^{(b)} + \pi\ \ \forall i \tag{4}$$

i.e. the locations of the minutiae are all the same while the orientations differ by π. Even if any minutiae matcher would mismatch this these two sets, according to [11], they would have the same template. It is well known in fact that:

$$|\mathscr{M}(\omega_x,\omega_y)|^2 = \mathscr{F}\{M(x,y)\otimes M(x,y)\} \tag{5}$$

being $\otimes$ the cross-correlation operator. Since the cross-correlation depends only on the relative phase difference between signals, it is clear that both $M^{(a)}$ and $M^{(b)}$ have equal autocorrelation.

B. Sparse Cross-correlation in the Continuous Spatial Domain

In this section we show how to use the complex minutiae representation (1) to design a matcher working directly in the spatial domain. Given a pair of minutiae sets $M^{(a)}$ and $M^{(b)}$, their cross-correlation is defined as:

$$\begin{aligned}C^{(a,b)}(x,y) &= M^{(a)}(x,y)\otimes M^{(b)}(x,y) = \\ &= G(x,y) * \Delta^{a,b}(x,y)\end{aligned} \tag{6}$$

where

$$G(x,y) = \frac{1}{2\pi 2\sigma^2}e^{\frac{-(x^2+y^2)}{4\sigma^2}} \tag{7}$$

and

$$\Delta^{a,b}(x,y) = \sum_{i=1}^{N^a}\sum_{j=1}^{N^b} e^{\iota\left(\alpha_i^{(a)}-\alpha_j^{(b)}\right)}\delta\left[x-\left(x_i^{(a)}-x_j^{(b)}\right),y-\left(y_i^{(a)}-y_j^{(b)}\right)\right] \tag{8}$$

Actually, ridge endings and bifurcations need to be treated separately. Therefore, we divide the minutiae set into disjoint subsets M_{end} and M_{bif}, compute the cross-correlation between homologous sets and sum them:

$$C_{tot}^{(a,b)}(x,y) = C_{end}^{(a,b)}(x,y) + C_{bif}^{(a,b)}(x,y). \tag{9}$$

The similarity score is given by the maximum value of the real part of the suitably normalised cross-correlation:

$$S\left(M^{(a)},M^{(b)}\right) = \frac{8\pi\sigma^2}{N_a+N_b}\max_{x,y}\left(\mathscr{R}e\left\{C_{tot}^{(a,b)}(x,y)\right\}\right) \tag{10}$$

where $\mathscr{R}e\{\cdot\}$ represents the real value. The normalisation value is chosen so that the matching score between identical minutiae sets is approximately 1 (it is exactly 1 when $\sigma\to 0$). It is worth mentioning that no hard decision is made on the correspondence between a minutia pair, and the strength of each minutia similarity is kept for the final decision. As we will see in Section III, this makes the method robust to missing-minutiae scenario.

The computation of (8) is straightforward since we just need to compute all the possible differences between minutiae:

$$\begin{aligned}C^{(a,b)} = \Big\{\Big(&x_i^{(a)}-x_j^{(b)}, y_i^{(a)}-y_j^{(b)}, \alpha_i^{(a)}-\alpha_j^{(b)}\Big)\Big\} \\ &|i=1,...N^a, j=1,...N^b\end{aligned} \tag{11}$$

It is worth pointing out that this step is identical to what the majority of minutiae-based fingerprint matcher does. We will refer to (11) as minutiae set cross-correlation.

On the other hand, the full computation of the evenly sampled version of (6) would be quite computationally expensive since the evaluation of each point of the cross-correlation function underlines the computation of $N_{end}^a\cdot N_{end}^b + N_{bif}^a\cdot N_{bif}^b$ steps. Nevertheless, because of the sparsity of $C^{(a,b)}(x,y)$, and since we are interested only in estimating its maximum value, we can evaluate the values of $C^{(a,b)}(x,y)$ just in the set correlation points defined in (11), i.e.:

$$\begin{aligned}\widehat{C}^{(a,b)}(x,y) &= C_{tot}^{(a,b)}(x,y)\cdot 1_C(x,y) \\ C &= C_{end}^{(a,b)}\cup C_{bif}^{(a,b)}\end{aligned} \tag{12}$$

ISBN 978-90-827970-1-5

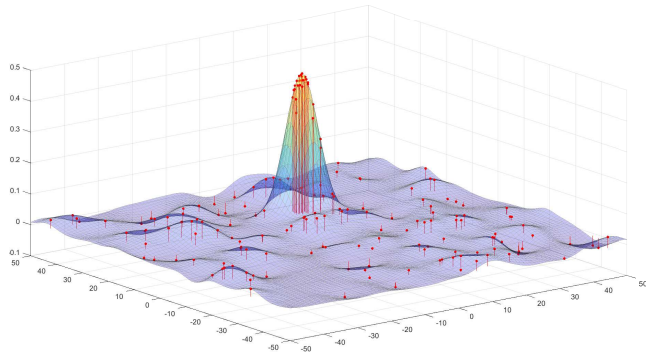

Fig. 2. Continuous spatial cross-correlation between complex minutiae $C^{(a,b)}(x,y)$ and sampled version $\widehat{C}^{(a,b)}(x,y)$.

where $1_C(x,y)$ is the Indicator function:

$$1_A(x,y) = \begin{cases} 1 & \text{if } (x,y) \in A \\ 0 & \text{otherwise.} \end{cases} \tag{13}$$

It is sufficient to calculate the value of the cross-correlation in those points since the sought maximum is located next to highest aggregation of points from the C set. In other words, the spatial resolution of the sampled cross-correlation $\widehat{C}^{(a,b)}(x,y)$ grows with the value of $C^{(a,b)}(x,y)$. An example of this behaviour can be seen in Figure 2. The number of steps to compute $\widehat{C}^{(a,b)}(x,y)$ is thus $\left[N^a_{end} \cdot N^b_{end} + N^a_{bif} \cdot N^b_{bif}\right]^2$. The number of values to compute can be further decreased by discarding the points too far from the origin. In summary, the sparsity of the signal representing the minutiae set (1) makes the complexity of the algorithm be $O\left(N^4\right)$ and independent to the resolution of x and y axis. Note that the computational complexity is the same of NIST's Bozorth3 [13].
The described algorithm does not take into account rotations of the minutiae sets. It is then required to explicitly apply a set of rotations to one of the minutiae sets and find the optimal one.

$$\begin{pmatrix} x_j^{(b)} \\ y_j^{(b)} \end{pmatrix} \leftarrow \begin{pmatrix} \cos\phi & -\sin\phi \\ \sin\phi & \cos\phi \end{pmatrix} \begin{pmatrix} x_j^{(b)} \\ y_j^{(b)} \end{pmatrix} \qquad \alpha_j^{(b)} \leftarrow \alpha_j^{(b)} - \phi \tag{14}$$

The maximization algorithm we used is based on golden section search and parabolic interpolation [14].

C. Frequency Fixed-Length Implementation

All the steps described in the previous section can be also implemented in frequency domain $\mathscr{M}(\omega_x,\omega_y) = \mathscr{F}\{M(x,y)\}$ where cross-correlation is given by:

$$\mathscr{C}^{a,b}(\omega_x,\omega_y) = \mathscr{M}^a(\omega_x,\omega_y)\mathscr{M}^b(\omega_x,\omega_y)^\star. \tag{15}$$

As we did before for the spatial implementation, we separate cross-correlation between homologous minutiae, i.e. ridge endings and bifurcation:

$$\mathscr{C}^{a,b}_{tot}(\omega_x,\omega_y) = \mathscr{C}^{a,b}_{end}(\omega_x,\omega_y) + \mathscr{C}^{a,b}_{bif}(\omega_x,\omega_y). \tag{16}$$

In order to find the matching score we should sample $\mathscr{C}^{a,b}_{tot}$, compute the Discrete Fourier Transform (DFT) and take the maximum value.

$$S\left(M^{(a)}, M^{(b)}\right) = \frac{2\,max\left(\mathscr{R}\left\{IFFT2\left[\mathscr{C}^{a,b}_{tot}[n,m]\right]\right\}\right)}{|<\mathscr{M}^a[n,m]>|^2 + |<\mathscr{M}^b[n,m]>|^2} \tag{17}$$

Since multiplications in the DFT domain correspond to a circular convolution in the spatial domain, in order to avoid aliasing effects, the sample rate in the frequency domain in ω_x (ω_y) direction should be chosen to be greater or equal to $2\frac{2\pi}{L}$, where L is the number of pixels in the x (y) direction. The maximum frequency to sample depends on the chosen σ value since it depends on which values (ω_x,ω_y) make $e^{-(\omega_x^2+\omega_y^2)\frac{\sigma^2}{2}}$ go close to zero. However, this implementation does not exploit the sparsity of the original signal in the spatial domain, since each minutia pulse is spread on the whole frequency domain, thus increasing the computational complexity. For this reason, various samples reduction techniques have been proposed [11]. Nevertheless, in this work, we have not dealt with this issue. Even though the spatial implementation is more computationally efficient, the frequency implementation exploits a fixed-length representation, that is a mandatory property for many biometric crypto-systems methods [2], [4].

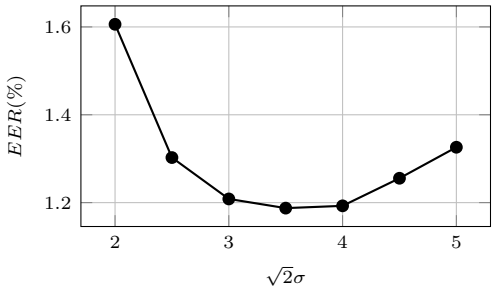

Fig. 3. EER vs σ

III. Implementation and Experimental Analysis

The proposed algorithms have been evaluated on the MCYT [15] database. Only fingers acquired with optical devices have been taken into account. We have used both left- and right-hand index and middle fingers from 100 users (0000 to 0099 IDs). Each finger has 12 realizations, 6 of which have been used for enrolment, 6 for verification. During the tests, only homologous fingers have been compared each other. Minutiae have been extracted through NIST's MINDTCT [13].

A remarkable characteristic of our method is that it has very few parameters to be defined: the σ parameter, the research window of optimal rotation, and the maximum number of rotations to try. The research window has been set to $\left(-\frac{\pi}{12}, \frac{\pi}{12}\right)$

ISBN 978-90-827970-1-5 © EURASIP 2018

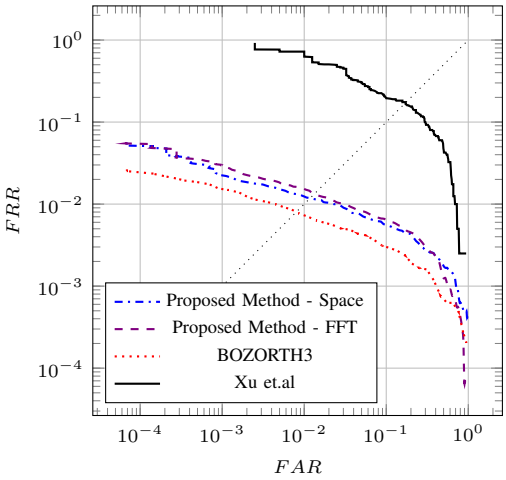

Fig. 4. ROC Curve

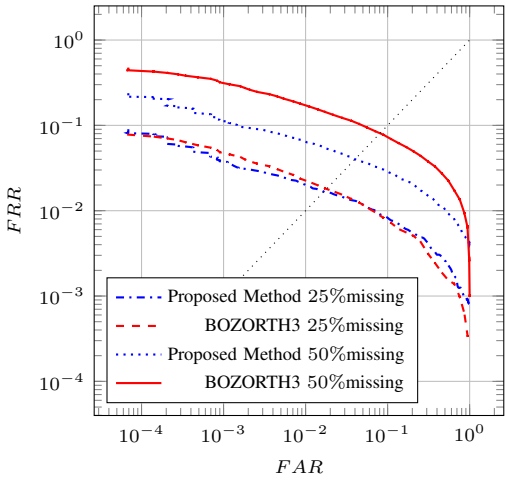

Fig. 6. ROC Curve in the case of missing-minutiae

while the maximum number of rotations has been set to 10 for computational reasons. Regarding σ, in Figure 3 the equal error rate (EER) for different values of σ is shown. Since $\sigma = \frac{3.5}{\sqrt{2}}$ shows the best performances, the following tests use this parameter.

In Figure 4, the ROC curves of both implementations of our method, the spectral minutiae method [11] and NIST's BOZORTH3 [13] are compared. While [11] method performance are very low for reasons explained in Section II-A, our method's performance are slightly below NIST's ones. Both our implementations show roughly the same performance. That is because they basically compute the same scores with different procedures. For this reason, in the following tests, only the spatial implementation will be evaluated since it is the fastest. In Figure 5, the scatter plot of the scores obtained from the comparison of corresponding minutiae is shown. We can notice that, even though the scores are well correlated, the spatial domain implementation gives slightly higher scores. That is probably because the spatial domain implementation is more accurate in estimating the maximum cross-correlation value (10) due to the sampling effects in the FFT implementation.

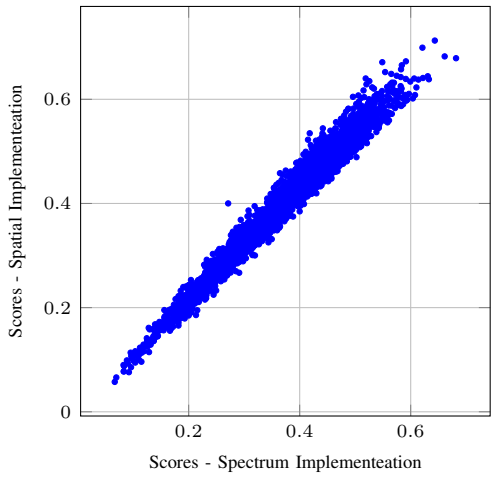

Fig. 5. Scatter plot of the scores computed through spatial and spectral implementations

Our approach has shown to be particularly robust when some minutiae are missing, such as in the case of small size acquisition device. We have simulated the aforementioned scenario by cropping the fingerprint images so that the minutiae are discarded. We took into account two different cases: $p = 25\%$ and $p = 50\%$ missing-minutiae. In order to remove $p\%$ of the minutiae, we randomly discarded minutiae falling below percentile p of x or y position, or above $(100 - p)\%$. We considered the scenario in which only the genuine probes have cropped images, while the enrolled fingers and the attacker probes have not been cropped. As a matter of fact, in a realistic scenario, both enrolment and attack processes are more accurate than everyday genuine users' identification attempts. As it can be seen in Figure 6, in the 25% missing-minutiae scenario, our method and the NIST's one show roughly the same performance, while our approach works remarkably better than Bozorth3 in the 50% missing-minutiae scenario. The robustness of our method is probably due to the fact that, contrary to Bozorth3, no hard decision is taken on the correspondence between single minutiae pairs. Therefore, even if few minutiae are available, if they are strongly similar to a subset of the reference fingerprint, the matching decision is correctly taken.

IV. Conclusion

In this paper, we have introduced a novel minutiae-based matching algorithm for fingerprint recognition built on an elegant and straightforward mathematical formulation. The method has shown to be more robust with cropped fingerprints compared with NIST's Bozorth3 method. We proposed two

ISBN 978-90-827970-1-5 © EURASIP 2018

different implementations. The first one is very computationally efficient while the second one makes use of a fixed length representation. We think that the simple mathematical closed form of the algorithm can be a solid starting point to develop further methods. For example, the spatial implementation may be integrated with fuzzy vault techniques, while the frequency implementation with fixed-length helper data schemes. The current drawback of our frequency representation is that it is not invariant to spatial translations and rotations that let the arrangement of a helper data scheme to be not straightforward.

ACKNOWLEDGMENT

We gratefully acknowledge the support of NVIDIA® Corporation with the donation of the Titan Xp™ GPUs used for this research.

REFERENCES

[1] D. Peralta, M. Galar, I. Triguero, D. Paternain, S. García, E. Barrenechea, J. M. Benítez, H. Bustince, and F. Herrera, "A survey on fingerprint minutiae-based local matching for verification and identification," *Inf. Sci.*, vol. 315, no. C, pp. 67–87, 2015.

[2] G. E. Hine, E. Maiorana, and P. Campisi, "A zero-leakage fuzzy embedder from the theoretical formulation to real data," *IEEE Transactions on Information Forensics and Security*, vol. 12, no. 7, pp. 1724–1734, 2017.

[3] K. Nandakumar and A. K. Jain, "Biometric template protection: Bridging the performance gap between theory and practice," *IEEE Signal Processing Magazine*, vol. 32, no. 5, pp. 88–100, Sept 2015.

[4] M. Gomez-Barrero, J. Fiérrez, J. Galbally, E. Maiorana, and P. Campisi, "Implementation of fixed-length template protection based on homomorphic encryption with application to signature biometrics," *2016 IEEE Conference on Computer Vision and Pattern Recognition Workshops (CVPRW)*, pp. 259–266, 2016.

[5] H. Xu, R. N. J. Veldhuis, A. M. Bazen, T. A. M. Kevenaar, T. A. H. M. Akkermans, and B. Gokberk, "Fingerprint verification using spectral minutiae representations," *IEEE Transactions on Information Forensics and Security*, vol. 4, no. 3, pp. 397–409, Sept 2009.

[6] A. K. Jain, S. Prabhakar, L. Hong, and S. Pankanti, "Fingercode: a filterbank for fingerprint representation and matching," in *Proceedings. 1999 IEEE Computer Society Conference on Computer Vision and Pattern Recognition (Cat. No PR00149)*, vol. 2, 1999, p. 193 Vol. 2.

[7] R. Cappelli, M. Ferrara, and D. Maltoni, "Minutia cylinder-code: A new representation and matching technique for fingerprint recognition," *IEEE Transactions on Pattern Analysis and Machine Intelligence*, vol. 32, no. 12, pp. 2128–2141, Dec 2010.

[8] W. Lee, S. Cho, H. Choi, and J. Kim, "Partial fingerprint matching using minutiae and ridge shape features for small fingerprint scanners," *Expert Systems with Applications*, vol. 87, pp. 183 – 198, 2017.

[9] O. Zanganeh, B. Srinivasan, and N. Bhattacharjee, "Partial fingerprint matching through region-based similarity," in *2014 International Conference on Digital Image Computing: Techniques and Applications (DICTA)*, Nov 2014, pp. 1–8.

[10] K. Nandakumar and A. K. Jain, "Local correlation-based fingerprint matching," in *In Indian Conference on Computer Vision, Graphics and Image Processing*, 2004, pp. 503–508.

[11] H. Xu and R. N. J. Veldhuis, "Complex spectral minutiae representation for fingerprint recognition," in *2010 IEEE Computer Society Conference on Computer Vision and Pattern Recognition - Workshops*, June 2010, pp. 1–8.

[12] H. Xu and R. Veldhuis, *Spectral Minutiae Representations for Fingerprint Recognition*. IEEE Computer Society, 2010, pp. 341–345.

[13] C. Watson, M. Garris, E. Tabassi, C. Wilson, S. Janet, and K. Ko, "Users guide to export controlled distribution of nist biometric image software (nbis-ec)."

[14] R. Brent, *Algorithms for Minimization Without Derivatives*, ser. Dover Books on Mathematics. Dover Publications, 1973.

[15] J. Ortega-Garcia, J. Fierrez-Aguilar, D. Simon, J. Gonzalez, M. Faundez-Zanuy, V. Espinosa, A. Satue, I. Hernaez, J. J. Igarza, C. Vivaracho, D. Escudero, and Q. I. Moro, "Mcyt baseline corpus: a bimodal biometric database," *IEE Proceedings - Vision, Image and Signal Processing*, vol. 150, no. 6, pp. 395–401, Dec 2003.